Disorder-induced resonant tunneling in planar quantum-dot nanostructures

D. Jovanovic* and J. P. Leburton
Beckman Institute for Advanced Science and Technology, University of Illinois, Urbana, Illinois 61801

H. Chang, R. Grundbacher, and I. Adesida
Center for Compound Semiconductor Microelectronics, University of Illinois, Urbana, Illinois 61801
(Received 3 March 1994)

Planar quantum-dot nanostructures have been shown to exhibit resonant features in their near-threshold conductance characteristics. However, the data often display strong nonuniformity in peak amplitude and a lack of reproducibility between devices, which suggests the presence of an influential disorder mechanism. In the present investigation, we perform a three-dimensional numerical analysis of structural disorder in a thin-gated quantum-dot nanostructure. The experimental conductance data for this device exhibit robust resonant features above $T=4.2$ K despite the presence of extremely wide tunneling barriers. A self-consistent simulation of the device in the virtual-crystal approximation shows no resonant features in the I-V characteristic, thereby excluding any direct influence of the quantum dot. Activating structural disorder in the simulation via interface and surface roughness, however, gives rise to resonant features that strongly resemble the experimental data. We thereby demonstrate that disorder mechanisms in planar nanostructures have a profound influence on near-threshold carrier transport to the extent that they may dominate the effects of intentionally fabricated confinement features.

I. INTRODUCTION

In the last few years, there have been numerous investigations of near-threshold resonant tunneling through molecular-beam-epitaxy (MBE)-grown planar quantum-dot nanostructures. These devices have generated significant interest because they exhibit strong Coulomb-blockade effects[1] and show promise for robust resonant-tunneling applications. Although analytical[2,3] and numerical[4] models have successfully explained the periodic conductance peaks observed at cryogenic temperatures, several features of the experimental data have not been analyzed in detail and their explanation to date remains inconclusive. Specifically, the nonmonotomic increase of the conductance amplitudes with gate bias implies the presence of some type of disorder, which influences the transport properties of the structure. This possibility was initially explored in the analytic model of Meir, Wingreen, and Lee[3] who phenomenologically introduced variations in resonant linewidths Γ and reproduced a nonmonotonic peak variation. A self-consistent numerical analysis of this device[4] in the virtual-crystal approximation (VCA), i.e., by assuming perfect surfaces and $Al_{0.3}Ga_{0.7}As$ interfaces, and neglecting disorder, revealed an exponential monotonic growth of Γ with increasing gate bias. Since the experimental data exhibit a much more gradual albeit nonmonotonic envelope, they appear likely due to an unscreened disorder mechanism (i.e., interface roughness) which activates transmission through the tunnel barriers and accounts for the disparity between the experimental and numerical data. Other lateral resonant-tunneling quantum-dot devices are characterized by a similar series of randomly varying resonant peak amplitudes,[5] which typically show no correlation from device to device.[6] The suggestion that the near-threshold transport properties of these devices are dominated by intentionally fabricated features is, therefore, in serious doubt and the more likely explanation is that each resonant structure is derived from the disorder potential as in single-barrier devices.[7,8]

Various experimental investigations have characterized the nature of structural imperfections, which arise during material growth and processing. Holonyak *et al.*[9] have shown that slow epitaxial-growth processes [i.e., MBE and metal-organic chemical-vapor deposition] with sharp on-off control display an inherent lack of stoichiometric control near a heterointerface on the order of one or two monolayers in the growth direction. The disorder is laterally manifested in the form of interface clusters, which result from the diffusion and desorption of alloy constituents over the growth plane.[10] A direct characterization of heterointerface quality is possible with exciton photoluminescence (PL) techniques as discussed by Herman, Bimberg, and Christen.[11] Their data illustrate the presence of large-scale interfacial macrocluster formation with a lateral extent in excess of 1-μm GaAs-$Al_{0.3}Ga_{0.7}As$ quantum wells. The resolution of PL measurements, however, is limited by the size of the induced exciton, which is typically in the range of 5–10 nm. A probe of the microscopic structure of interface roughness in GaAs-$Al_{0.3}Ga_{0.7}As$ quantum wells has recently been performed by Johnson *et al.*[12] using scanning tunneling microscopy. Their data are accurate to within atomic precision and reveal interfacial roughness on the order of 1–10 monolayers in both the perpendicular and lateral directions even in high-mobility samples. This type of interface disorder is generated by inherent variations in Al mole fraction in the ternary $Al_{0.3}Ga_{0.7}As$ layer. Surface roughness and impurity disorder in doping layers are also present in varying degrees depending on the specific de-

vice configuration. The topology of an exposed surface has long-range influence on a quantization potential via random fluctuations in the location of Fermi-level pinning. In addition, the spatial variations of impurity atoms in a doping layer have been shown to give rise to pronounced structure in the confined regions of modulation-doped devices.[13] The combined effect of all these disorder mechanisms may result in a distortion of the desired confining potential in a particular geometry, which can lead to significant deviations from intended device performance.

Numerous theoretical investigations have been undertaken to study the strength and impact of disorder in various device geometries. Catellani and Ballone[14] have demonstrated that the introduction of islands with $\pm$ one-monolayer depth at the interfaces of double quantum wells gives rise to energy shifts and line shapes that closely resemble the measured optical spectra. An analysis of MBE-grown vicinal quantum wires by Taylor *et al.*[15] reveals a significant distortion of the one-dimensional (1D) density of states in the presence of interface disorder when compared to the predicted ideal behavior. A similar analysis by Singh[16] suggests that even if the overall distortion of the 1D density of states is suppressed, a large fraction of the low-energy states experiences localization and that carrier transport, which inherently samples the long-range behavior of the wave functions, should be significantly altered. Furthermore, the comprehensive work of Davies and Nixon and co-workers[13,17] reveals the significant potential fluctuations, which result from unscreened randomly distributed dopants in modulation-doped devices. Their analysis goes so far as to calculate the conductance through a point contact and demonstrates the degradation of conductance plateaus for various disordered dopant configurations.

The purpose of the present investigation is to analyze the transport characteristics of an MBE-grown lateral single-gated quantum-dot device and assess the degree to which structural disorder affects its transport properties. The transport characteristics of the device display anomalous conductance fluctuations[6] despite the presence of relatively wide tunnel barriers. To analyze the influence of structural disorder, we perform a numerical simulation of the device with a self-consistent 3D Schrödinger-Poisson[4] approach similar to that used for investigating the single electron transfer device conceived by Meirav *et al.*[1] Structural disorder in the form of interface and surface roughness is added in varying degrees to gauge how the transport characteristics are transformed from the VCA to a disorder dominated system. Although the rigorous theoretical investigation of ionized dopant randomization by Davies and Nixon and co-workers[13,17] leaves no doubt of its importance, we omit this disorder mechanism due to difficulties in capturing its essential features with a coarse computational mesh. Instead, we will show that interface and surface roughness are sufficient to account for the resonant-transport features observed in the experimental devices. Our results can be generalized to other disorder mechanisms (i.e., ionized dopant randomization), which are not directly included in our model but which undoubtedly contribute to quantum transport in an analogous fashion.

II. EXPERIMENTAL DEVICE

The experimental device examined here is a thin-gated mesa-etched quantum-dot nanostructure. A cross section of the device and a set of theoretical potential energy contours are shown in Fig. 1. Briefly, the heterostructure was grown by MBE on an undoped GaAs substrate. A 1-μm-thick GaAs buffer layer was grown on the substrate followed by a 17.5-nm undoped $Al_{0.3}Ga_{0.7}As$ spacer, a Si δ doping of 5×10^{12} cm^{-2}, a 20-nm layer of $Al_{0.3}Ga_{0.7}As$, and a 20-nm n^+-GaAs cap layer. Hall measurements on the sample indicated a sheet carrier density of $N_s=4.7\times10^{11}$ cm^{-2} and a mobility of $\mu_s=5.0\times10^5$ cm^2/V s at $T=4.2$ K. Isolation and contact patterning were then carried out by optical lithography followed by a wet etch. Ohmic contacts to the source/drain were made with alloyed AuGe/Ni/Au. A source-drain separation of 20 μm was chosen to allow relaxation of hot electrons injected from the source. The n^+-GaAs cap was then removed from the heterostructure surface by selective wet etching. High-resolution *e*-beam lithography was used to define the Poly-Methyl-Methacrylate (PMMA) resist for the quasi-1D mesa followed by a wet etch in H_3PO_4:H_2O_2:H_2O. Despite the better resolution

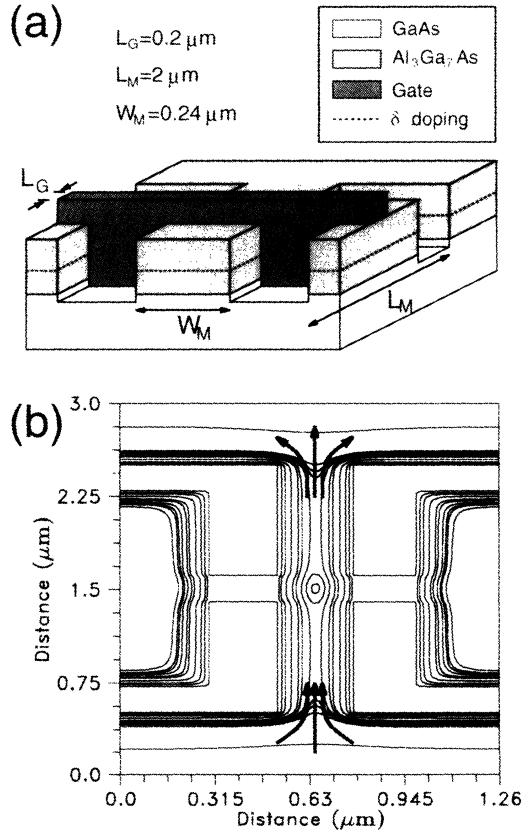

FIG. 1. (a) Schematic configuration for the experimental planar thin-gated quantum-dot device. (b) Potential contours calculated in a plane just below the GaAs-$Al_{0.3}Ga_{0.7}As$ interface. The arrows indicate the direction of current flow.

of dry etching, a wet etch was chosen in an effort to minimize surface damage. Finally, the thin gate was defined using e-beam lithography followed by Ti/Au lift off. Devices with quasi-1D channel widths ranging from 0.15 to 0.7 μm were fabricated and a 0.24-μm channel width was found to give the best threshold behavior. Wider channels operated in a depletion mode whereas narrower mesas resulted in a completely cut off channel. The 200-nm thin-gate length was modulated with a positive gate bias, which induced the third dimension of confinement and formed a quantum dot in the quasi-1D channel below the gate.

A set of I-V characteristics of this device is shown in Fig. 2 for various drain-source biases, V_{DS}. The measurements were conducted at $T=4.2$ K and the samples were cooled without illumination to avoid persistent currents resulting from DX center activation. The gate bias, V_G was swept while V_{DS} was fixed to values ranging from 0.1 to 1 mV. The predominant features in the conductance are independence of the threshold voltage from V_{DS} and the conductance peaks that persist beyond $V_{DS}=1$ mV. Both of these features point to resonant tunneling as the predominant mechanism for controlling the near turn-on I-V characteristic. However, the presence of resonant features is rare in the device population and, when present, exhibits a strong lack of uniformity in peak amplitude and periodicity from sample to sample. The case for resonant tunneling can be made simply with a qualitative examination of the confinement geometry of the device. The application of a positive V_G forms the quantum dot in the quasi-1D channel by locally lowering the potential energy underneath the gate. The remaining portions of the quasi-1D channel retain a higher potential energy and, therefore, form barriers separating the quantum dot from the contacts [see Fig. 1(b)]. A positive sweep of V_G gradually lowers the height of quasi-1D barriers and results in the eventual activation of conduction. In addition, a positive gate-bias sweep results in an enhancement of the quantum-dot charge density and the generation of multiple resonant conditions between the quantum-dot eigenenergies and the Fermi energy in the contacts, E_F. Undoubtedly, Coulomb-blockade effects are also present and play a role in determining the conductance characteristics. However, this simple model fails to explain the relatively sparse number of experimental devices that exhibit near-resonant characteristics or the large fluctuations in peak height and periodicity. In addition, inspection of the device dimensions reveals that the quasi-1D barriers should be on the order of $\simeq 500$ nm-1 μm wide and, therefore, relatively impermeable to tunneling, except over a few tenths of μeV from the very tip of the barrier. For higher barriers or lower carrier energy, the resonance transmission is too sharp and too narrow to withstand a realistic thermal broadening of more than a few mK. Clearly, a randomizing agent is present in the device population and responsible for the lack of uniformity in the I-V characteristics. This randomness can be accounted for by interface disorder and surface roughness, both of which are inherent properties of material growth and processing. It might be counterintuitive to invoke surface and interface roughness to explain the oscillatory structures in the I-V characteristics of high-mobility materials when it is known that impurity scattering due to random dopants is a significant limiting factor for low-temperature mobility in mesoscopic devices. However, structural disorder which manifests on a shorter range than impurity scattering, with fluctuations of the order of 1 meV in the barrier height, is sufficient to account for the experimental data, while the long-range influence of random dopant certainly contributes to the general trends observed in this work.

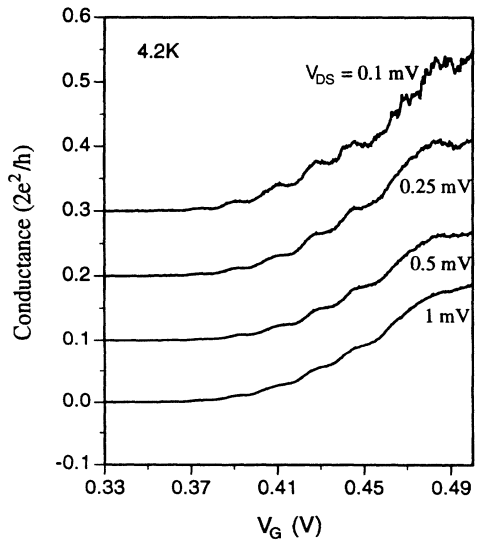

FIG. 2. Experimental conductance characteristics at $T=4.2$ K for a rare sample, which exhibits features of resonant tunneling. The various curves indicate the persistence of distinguishable resonant-tunneling characteristics beyond $V_{DS}=1.0$ mV.

III. THEORETICAL BACKGROUND

The analysis of structural disorder in semiconductor devices has traditionally been treated by representing crystalline imperfections as randomly distributed elastic-scattering centers. While this approach is well justified in bulk systems for which transport is inherently particle-like, quantized systems exhibit extended electronic states and require a nonlocal treatment of disorder. The manifestation of disorder-induced potential leads to weakly localized conducting channels through seemingly impenetrable barriers, which give rise to resonant-transport characteristics. To fully account for this behavior, structural disorder must be rigorously modeled and realistically encoded. The symmetry-breaking nature of a crystalline imperfection, therefore, implies that a 3D model is required to fully capture its essential properties. One such model developed by Ting, Kirby, and McGill[18] has been used to investigate the influence of interface roughness on transport perpendicular to a heterointerface. Their approach involves a 3D planar supercell simulation capable of rigorously treating transport in structurally confined quantized geometries. Their data clearly demonstrate the nonlocal influence of disorder via auxiliary peaks in the transmission coefficient for double-

barrier resonant-tunneling structures and structurally confined quantum wires. For the planar field-confined geometry analyzed here, interface and surface roughness play a prominent role since transport occurs parallel to the interface. In addition, field confinement and disorder screening require self-consistency between the potential and charge distributions.

Our theoretical model is based on a 3D self-consistent quantum-mechanical simulation of the electronic properties of the structure.[4] Briefly, the Schrödinger equation is solved using the iterative extraction-orthogonalization method[20] (IEOM), which enables the rapid evaluation of an arbitrary number of eigenstates in each quantized region of a particular device geometry. In the present device, we identify regions that exhibit 2D or 1D confinement and adiabatically solve 1D or 2D versions of the Schrödinger equation, respectively. Although a similar analysis has been used to treat 0D (quantum-dot) confinement rigorously with a full 3D solution of the Schrödinger equation,[4] this level of simulation would prove too costly in the present treatment since the weak disorder-induced localization would generate an enormous number of simulated 0D eigenstates. Instead, we treat the quantum dot as an extension of the 1D leads and draw on the efficiency of the 2D IEOM evaluation of the transverse wave functions to enhance the performance of the simulation. The accuracy of the 1D adiabatic approximation was previously tested against a rigorous 3D simulation of a 0D confined region in the VCS and good agreement was found between the respective eigenenergies, thereby validating its general use.[4] However, in the highly disordered systems encountered here, the rapid variation of the potential in all three dimensions casts doubt on the integrity of the adiabatic approximation. Nevertheless, in this investigation we are interested in capturing a qualitative understanding of the influence of structural disorder and the adiabatic approximation represents a reasonable tradeoff between theoretical rigor and execution time.

Once we obtain the relevant eigenstates in each region, they are assembled and weighted with the relevant statistical factor to obtain a device-wide 3D charge density. The charge density is then fed into a modified Newton-Raphson algorithm which implicitly solves Poisson's equation and drives the simulation towards self-consistency. We include exchange and/or correlation effects via the Kohn-Sham local-density approximation to account for high-order many-body effects at low temperatures. The computational mesh and boundary conditions are cast to accurately model the various material properties and overall 3D device geometry. Fermi-level pinning is imposed on all exposed surfaces to account for occupied surface states. This condition is modeled by establishing Dirichlet boundary conditions in the form of Schottky barriers ϕ_s on all surfaces except those under the gate, which are modified by the gate bias V_G via $\phi_s - qV_G$. Our choice for this surface model is based on its overall simplicity and computational efficiency despite the fact that it fails to account for the long-range Coulombic surface effects arising from the thin gate. Computational (unexposed) surfaces in our 3D grid are chosen such that they terminate in regions where bulk behavior occurs and are, therefore, suitably modeled by Neumann boundary conditions. A nonuniform mesh is used in the vertical (heterojunction) to allow refinement of the mesh width down to 5 Å to accurately model the disorder at the GaAs-$Al_{0.3}Ga_{0.7}As$ interface. The disorder is created by allowing interpenetration of GaAs mesh "tiles" into the $Al_{0.3}Ga_{0.7}As$ and vice versa. Mesh tiles of various lateral dimensions (200×200 Å^2, 800×800 Å^2, and 1600×1600 Å^2) are randomly assembled along the interface to create disordered interface clusters. Similarly, surface roughness is modeled by spatially varying the thickness of the surface boundary tiles over $\simeq 100$ nm. This approach results in a spatial variation of the Fermi-level pinning boundary condition, which subsequently generates long-range randomization of the confining potential. We note that both the disorder mechanisms in our model experience screening since they are treated self-consistently within our formalism.

IV. TRANSPORT

Once an equilibrium simulation is complete, the adiabatic multisubband quasi-1D eigenenergy is stored and subsequently used in the evaluation of transport characteristics. The eigenenergies are extended into the source regions by assuming that the transfer of electrons from the source into the lead also occurs adiabatically. Since the equilibrium simulation is somewhat computationally intensive ($\simeq 10$ h on a HP9000/735 workstation for each bias point), we run the code for several gate biases only and use IMSL interpolation routines on the adiabatic eigenenergies to obtain a quasicontinuous transconductance characteristic. At each interpolated gate bias, the transmission coefficient is evaluated from the interpolated adiabatic eigenenergy using a 1D transfer-matrix calculation. The justification of the adiabatic approximation is as follows. We first assume that the potential exhibits slow longitudinal variation giving rise to wave functions $\Psi(\mathbf{r})$, which are separable such that $\Psi(\mathbf{r})=\phi_m(x,y;z)\xi_n(z)$. Then, with the potential energy represented locally, the 3D Schrödinger equation reduces to

$$-\frac{\hbar^2}{2m^*}\nabla_z^2\xi_n(z)+E_m(z)\xi_n(z)=E_{m,n}\xi_n(z)\ , \tag{1}$$

where we assume that the z variation of $\phi_m(x,y;z)$ is negligible. The adiabatic quasi-1D eigenenergy $E_m(z)$ is obtained from the auxiliary equation

$$-\frac{\hbar^2}{2m^*}(\nabla_x^2+\nabla_y^2)\phi_m(x,y;z)+E_c(\mathbf{r})\phi_m(x,y;z) =E_m(z)\phi_m(x,y;z)\ , \tag{2}$$

which is solved in transverse planes (1D) down the longitudinal z axis of the computational grid. Once $E_m(z)$ is calculated at each interpolated gate bias, V_{DS} is phenomenologically superimposed and the transfer-matrix calculation is used to generate the transmission probability $|T(\epsilon)|^2$ over the relevant energy range. The finite tem-

perature current I is finally obtained by inserting $|T(\epsilon)|^2$ into the standard tunneling current formula[19]

$$I=\frac{2e^2}{h}\int d\epsilon |T(\epsilon)|^2[f(\epsilon)-f(\epsilon+V_{DS})] , \quad (3)$$

where e is the electron charge, h is Planck's constant, and $f(\epsilon)$ is the Fermi-Dirac distribution. To accurately treat the extremely narrow linewidths of the highly localized quantum-dot states, an iteratively focused search algorithm is performed around each resonance to within machine precision. This technique extracts resonances that would otherwise be missed by a uniform integration over the applicable energy range. The accuracy of the 1D adiabatic approximation was tested against a 2D recursive Green's function method and good agreement was demonstrated even for highly asymmetric confining potentials.[21] We note that although Coulomb-blockade effects were previously included in a similar VCA model,[4] they are omitted in the present simulation. The large number of resonances arising from the disorder-induced weak localization render the inclusion of charging effects too computationally expensive.

V. RESULTS AND DISCUSSION

Initially, we simulate the device in the VCA to determine whether the perfect device potential alone is sufficient to account for the resonant-tunneling features found in the experimental device characteristics. The adiabatic quasi-1D ground-state eigenenergy and I-V characteristics of the perfect device are shown in Fig. 3. The adiabatic quasi-1D eigenenergy [Fig. 3(a)] clearly exhibits the presence of a quantum dot in the vicinity of the thin gate and the formation of barriers in the quasi-1D channel, which separate the quantum dot from the 2D contact regions. In principle, electrons can tunnel through the active region only when interference effects in the quantum-dot cavity create standing waves (bound states) and thereby fulfill the resonance requirement. Although some degree of resonant tunneling should exist in the perfect device, the transport characteristics [Fig. 3(b)] show a complete lack of detectable structure in the device current. Examination of Fig. 3(a) reveals that the quasi-1D barriers are relatively flat and thick ($\simeq$500 nm). Since the barrier width is considerably larger than the electron Fermi wavelength, any transmission resonances through the structure should exhibit exceedingly narrow linewidths. The explanation for the structure-free I-V characteristics, therefore, follows by comparing the relative magnitudes of the tunneling component of the current to the thermionic-emission component. As V_G is increased, the long-range influence of the gate lowers the quasi-1D barriers and, therefore, monotonically enhances the thermionic-emission current at $T=4.2$ K. On the other hand, the tunneling current, which is superimposed on the thermionic-emission current, has a magnitude proportional to the resonant linewidth Γ when $kT \gg \Gamma$. Since the broad barriers in the perfect device lead to a set of Γ, which satisfy this condition, resonant tunneling contributes indistinguishably to the overall current and the transport characteristics in the VCA are completely

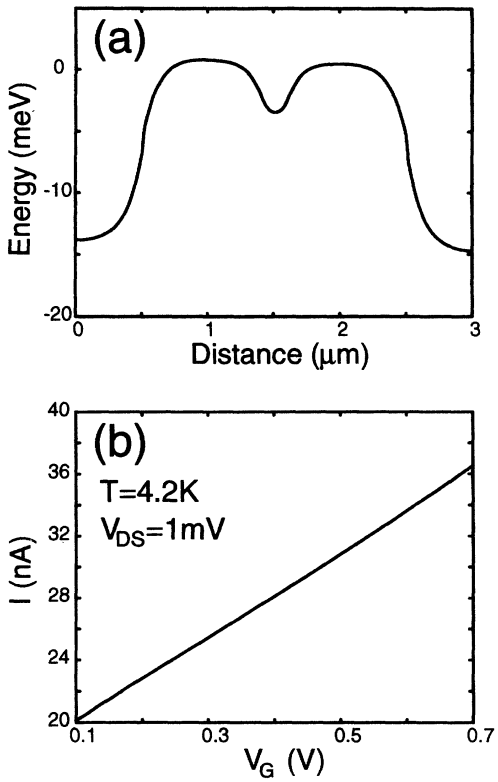

FIG. 3. (a) Adiabatic quasi-1D eigenenergy calculated for the device geometry in the VCA. (b) Transport characteristics indicate the absence of any structure in the current for perfect crystalline properties. The wide tunnel barriers ($\simeq$500 nm) create extremely narrow resonant linewidths, which do not influence electronic transport.

dominated by thermionic emission.

In the presence of disorder, weak localization in the barrier regions should significantly increase Γ for each resonance and thereby provide a discernible resonant-tunneling contribution to the overall current. To provide an initial examination into the influence of disorder, we have phenomenologically added highly localized repulsive barriers to the VCA adiabatic eigenenergy and reexamined the device transport properties. Figure 4 shows the modified adiabatic eigenenergy and the resulting I-V characteristics. Unlike the VCA result, the I-V characteristics for the modified structure exhibit strong resonant-tunneling behavior over a large range of V_G. Clearly, this phenomenological model demonstrates the potentially significant impact short-range disorder has on electronic transport in fabricated quantized devices.

To quantitatively assess the influence of realistic interface and surface roughness, we have introduced these disordered mechanisms into the 3D device geometry as described in Sec. III. Figure 5 shows a comparison of conduction-band surface plots in the VCA and in the presence of disorder. The plots are taken in the plane just below the GaAs-$Al_{0.3}Ga_{0.7}As$ interface and cover the entire active region of the device including the leads and contacts. The conduction-band energy in Fig. 5 scales with height and shading is used to discern subtle energy

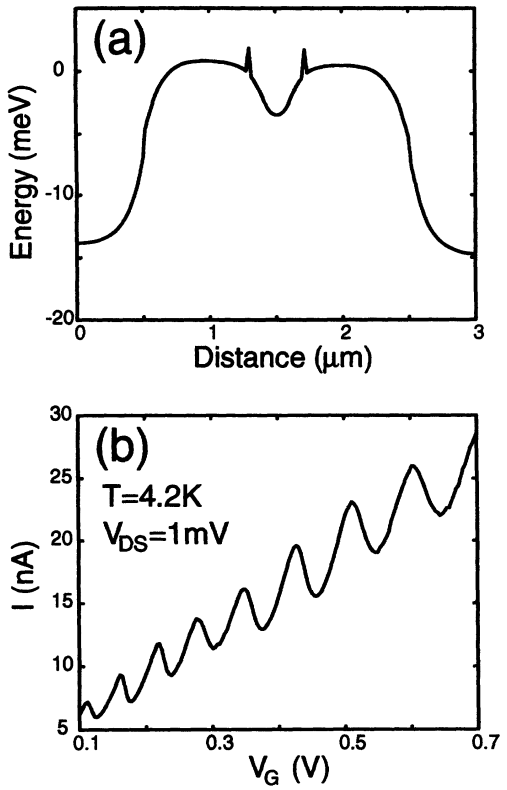

FIG. 4. (a) Adiabatic quasi-1D eigenenergy in the VCA with an artificially induced sharp repulsive barrier in the quasi-1D channel. (b) Transport characteristics show strong resonant-tunneling behavior and indicate that disorder may be an activating process for observing resonant-tunneling characteristics in quantized devices.

variations. The conduction band with disorder [Fig. 5(b)] clearly exhibits a mottled texture arising from the interface and surface roughness. Moreover, a comparison of Figs. 5(a) and 5(b) reveals that whereas the VCA simulation produces relatively thick uniform quasi-1D barriers, the disordered conduction band exhibits numerous islands of weak localization in the quasi-1D regions. The

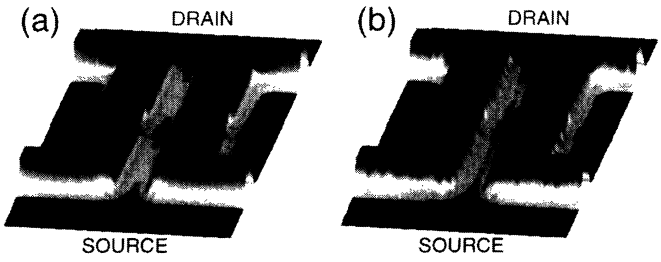

FIG. 5. Theoretical conduction-band surface plots calculated in a plane just below the GaAs-$Al_{0.3}Ga_{0.7}As$ interface (a) using the VCA and (b) with the presence of interface and surface disorder. The potential energy scales with the height of the surface and shading is used to discern subtle energy variations. The disordered surface clearly exhibits a mottled texture arising from the disorder and the presence of weakly localized regions in the quasi-1D channel, which activate resonant transport through the device.

net influence of weak localization is the effective narrowing of the tunneling length in quasi-1D barriers, which activates resonant transport through the device. Figure 6(a) shows the adiabatic eigenenergy corresponding to the disordered structure of Fig. 5(b). The disorder was produced by randomly assigning 200×200×5-Å^3 tiles at the heterointerface to either GaAs or $Al_{0.3}Ga_{0.7}As$ and randomly varying the position of the etched surface using 200×200×200-Å^3 boundary tiles. The influence of the disorder on the adiabatic eigenenergy is twofold. First, there is the vertical modulation of the potential, which provides an adiabatic shift of the local eigenenergy. In addition, the transverse modulation, largely due to surface roughness, causes local fluctuations of a few meV in the confinement strength, which are manifest as peaks and valleys in the adiabatic quasi-1D eigenenergy. Clearly, these potential fluctuations are mostly influential at the top of the barrier where they cannot be screened by the carriers and are consequently relevant for tunneling. In addition, the random nature of the potential results in a spectrum of narrowly and irregularly spaced eigenstates with significantly broadened transmission resonances. Qualitatively, the disordered potential reduces the effective barrier width and enables robust tunneling several meV below the maximum energy in an otherwise classical barrier.

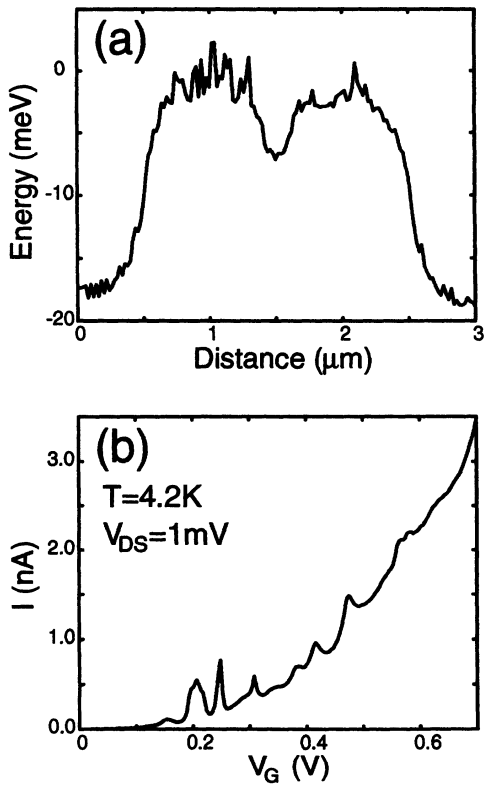

FIG. 6. (a) Adiabatic quasi-1D eigenenergy arising from structural disorder in the 3D device geometry. Interface clusters are randomly built from 200×200×5-Å^3 tiles at the GaAs-$Al_{0.3}Ga_{0.7}As$ interface. Surface disorder occurs over 200×200×200-Å^3 boundary tiles. (b) I-V characteristics indicate the presence of pronounced resonant-tunneling behavior.

The impact of the disorder is immediately apparent on the theoretical I-V characteristic shown in Fig. 6(b) which, contrary to simulations in the VCA, exhibits strong resonant-tunneling features near threshold at $T=4.2$ K. As V_G is swept to higher values and the quasi-1D barriers are lowered, the thermionic-emission component of the current begins to dominate and the resonant features are gradually diminished. The effect of varying the size of the interface clusters is shown in Figs. 7 and 8. The investigated interface tile sizes are $800\times800\times5$ Å^3 (Fig. 7) and $1600\times1600\times5$ Å^3 (Fig. 8) in addition to the $200\times200\times5$ Å^3 of Fig. 6. In all cases, the same surface disorder profile ($200\times200\times200$ Å^3) was used. The larger disorder data in Fig. 7 exhibit a reduction in the rapid variation in the adiabatic quasi-1D eigenenergy over that in Fig. 6 and correspondingly less resonant-tunneling features in the I-V characteristic. Nevertheless, near-threshold oscillations persist and more closely resemble the typical experimental transport data in Fig. 2. The coarsest interface disorder data (Fig. 8) show the least structure in the adiabatic quasi-1D eigenenergy. The primary disorder mechanism in Fig. 8 is surface roughness which, owing to long-range screening, results in a more gradual variation of the adiabatic eigenenergy. This is reflected in the very subtle resonant features in the conductance characteristic of Fig. 8.

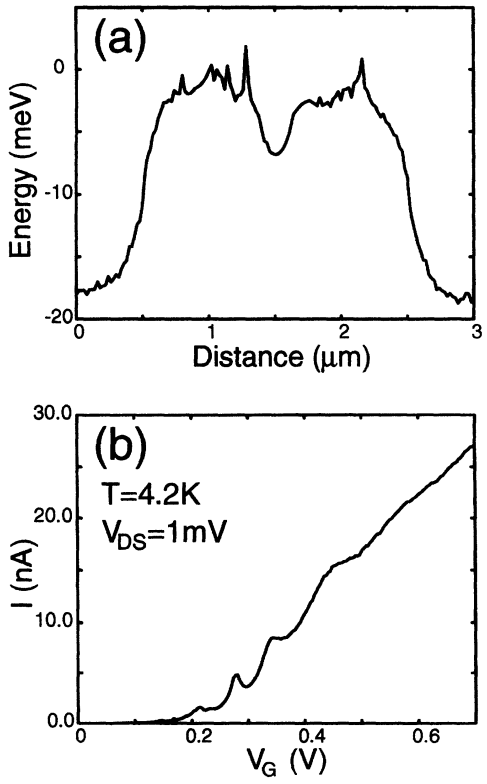

FIG. 7. (a) Adiabatic quasi-1D eigenenergy arising from structural disorder in the 3D device geometry. Interface clusters are randomly built from $800\times800\times5$-Å^3 tiles at the GaAs-$Al_{0.3}Ga_{0.7}As$ interface. Surface disorder occurs over $200\times200\times200$-Å^3 boundary tiles. (b) I-V characteristics indicate the presence of resonant-tunneling behavior.

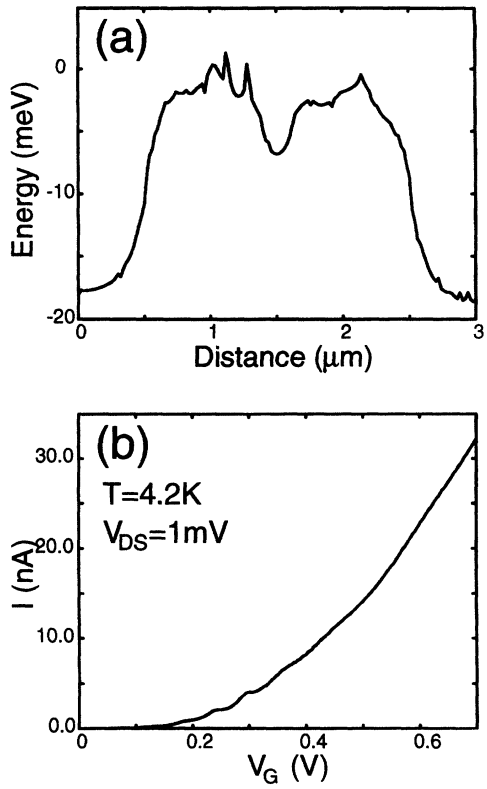

FIG. 8. (a) Adiabatic quasi-1D eigenenergy arising from structural disorder in the 3D device geometry. Interface clusters were randomly built from $1600\times1600\times5$-Å^3 tiles at the GaAs-$Al_{0.3}Ga_{0.7}As$ interface. Surface disorder occurred over $200\times200\times200$-Å^3 boundary tiles. (b) I-V characteristics indicate the presence of subtle resonant tunneling behavior.

These data suggest that interface irregularities on the order of 500–1500 Å are the most likely explanation for the resonant-tunneling features found in the experimental device.

To investigate the influence of V_{DS} variations on the conductance, we have run various simulations at $T=4.2$ K with $800\times800\times5$-Å^3 interface disorder and displayed the results in Fig. 9. The V_{DS}-induced broadening has

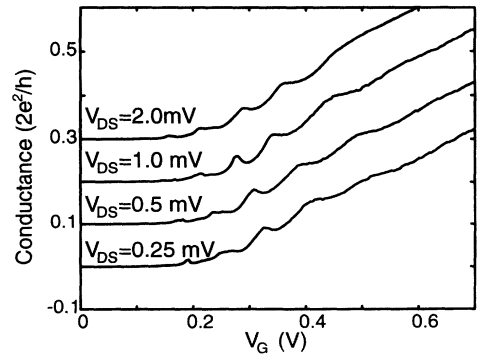

FIG. 9. Theoretical conductance characteristics with V_{DS} as a parameter at $T=4.2$ K. Interface clusters are randomly built from $800\times800\times5$-Å^3 tiles at the GaAs-$Al_{0.3}Ga_{0.7}As$ interface. Surface disorder occurs over $200\times200\times200$-Å^3 boundary tiles.

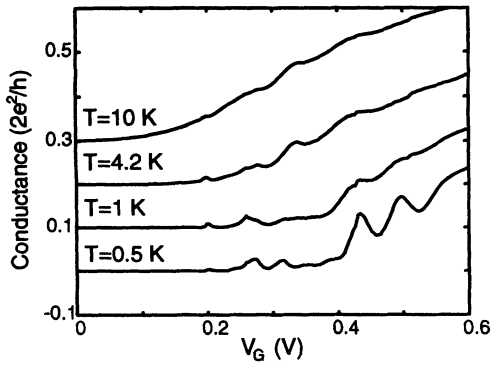

FIG. 10. Theoretical conductance characteristics with temperature as a parameter for $V_{DS}=0.1$ mV. Interface clusters are randomly built from $800\times800\times5$-Å^3 tiles at the GaAs-$Al_{0.3}Ga_{0.7}As$ interface. Surface disorder occurs over $200\times200\times200$-Å^3 boundary tiles.

little influence on the conductance in the linear response regime ($V_{DS}<kT$). Under this condition, thermal broadening dominates and the conductance shows little modification with decreasing V_{DS}. However, as V_{DS} is increased beyond kT, the V_{DS}-induced broadening begins to dominate and eventually smears the resonant peaks. Figure 9 shows that the resonant conductance peaks retain good resolution beyond $V_{DS}=1$ mV at $T=4.2$ K, which is confirmed by the experimental data in Fig. 2. The influence of temperature variation is exhibited in Fig. 10, which shows the conductance at various temperatures while $V_{DS}=0.1$ mV. The curve at $T=0.5$ K shows the strongest structure in the conductance and most closely resembles the bare transmission coefficient through the device. As the temperature is increased, the thermal broadening softens the resonant behavior and modifies the threshold voltage due to the onset of thermionic emission. Some resonant features remain up to $T=10$ K indicating the relative robustness of the disorder-induced resonant tunneling. We should emphasize that although our theoretical approach involving the adiabatic quasi-1D eigenenergy encapsulates the 3D nature of disorder into a simple 1D form, the transmission characteristics we calculate can be found in any appropriately disordered system, which qualitatively validates our model. Moreover, the disorder-induced near-threshold resonant behavior we have investigated has been repeatedly observed in planar modulation-doped nanostructures.

VI. CONCLUSION

In this investigation, we have demonstrated that disorder mechanisms play a prominent role in determining near-threshold conductance characteristics in quantum-dot nanostructures. This conclusion supports our earlier conjecture[4] that disorder has a prominent role in activating transport in certain Coulomb-blockade devices.[1] While our simulations indicate that interface and surface roughness alone can explain anomalous resonant-tunneling features, other disorder mechanisms (i.e., disorder in the impurity layer) are undoubtedly present in fabricated devices and contribute to the general trends we have observed. It is worth mentioning that most of the lateral quantum-dot nanostructures that have been realized to date exhibit relatively weak confinement potentials, which are easily dominated by inherent disorder-induced fluctuations for $T\leq10$ K. As fabrication techniques improve and lead to higher temperature operation, disorder-induced potential fluctuations will become insignificant, thereby enabling a practical resonant-tunneling-device technology.

ACKNOWLEDGMENTS

This work was supported by NSF Grant No. ECS 91-20641 and the Joint Services Electronics Program. One of the authors (D.J.) would like to thank Texas Instruments Inc. for providing the resources necessary to complete this manuscript.

*Present address: Central Research Laboratory, Texas Instruments Inc., P.O. Box 655936, MS134, Dallas, TX 75265.

[1] U. Meirav, M. A. Kastner, and S. J. Wind, Phys. Rev. Lett. **65**, 771 (1990); U. Meirav, P. L. McEuen, M. A. Kastner, E. B. Foxman, A. Kumar, and S. J. Wind, Z. Phys. B **85**, 357 (1991).

[2] C. W. J. Beenakker, Phys. Rev. B **44**, 1646 (1991).

[3] Y. Meir, N. S. Wingreen, and P. A. Lee, Phys. Rev. Lett. **66**, 3048 (1991).

[4] D. Jovanovic and J. P. Leburton, Phys. Rev. B **49**, 7474 (1994).

[5] Y. Wang and S. Y. Chou, Appl. Phys. Lett. **63**, 2257 (1993).

[6] H. Chang *et al.* (unpublished).

[7] S. Washburn, A. B. Fowler, H. Schmid, and D. Kern, Phys. Rev. B **38**, 1554 (1988).

[8] T. E. Kopley, P. L. McEuen, and R. G. Wheeler, Phys. Rev. Lett. **61**, 1654 (1988).

[9] N. Holonyak, W. D. Laidig, M. D. Camras, H. Morkoç, T. J. Drummond, K. Hess, and M. S. Burroughs, J. Appl. Phys. **52**, 7201 (1981).

[10] T. D. Lowes and M. Zinke-Allmang, J. Appl. Phys. **73**, 4937 (1993).

[11] M. A. Herman, D. Bimberg, and J. Christen, J. Appl. Phys. **70**, R1 (1991).

[12] M. B. Johnson, U. Maier, H.-P. Meier, and H. Salemink, J. Cryst. Growth **127**, 1077 (1993).

[13] J. H. Davies and J. A. Nixon, Phys. Rev. B **39**, 3423 (1989).

[14] A. Catellani and P. Ballone, Phys. Rev. B **45**, 14 197 (1992).

[15] J. P. G. Taylor, K. J. Hugill, D. D. Vvedensky, and A. MacKinnon, Phys. Rev. Lett. **67**, 2359 (1993).

[16] J. Singh, Appl. Phys. Lett. **59**, 3142 (1991).

[17] J. A. Nixon, J. H. Davies, and H. U. Baranger, Phys. Rev. B **43**, 12 638 (1991); M. J. Laughton, J. R. Barker, J. A. Nixon, and J. H. Davies, Phys. Rev. B **44**, 1150 (1991).

[18] D. Z.-Y. Ting, S. K. Kirby, and T. C. McGill, in *Proceedings of the International Workshop on Computational Electronics,* edited by C. R. Snowden and M. J. Howes (University of Leeds, Leeds, England, 1993).

[19] R. Landauer, Philos. Mag. **21**, 863 (1970).

[20] R. Kosloff and H. Tal-Ezer, Chem. Phys. Lett. **127**, 223 (1986).

[21] M. Macucci (private communication).

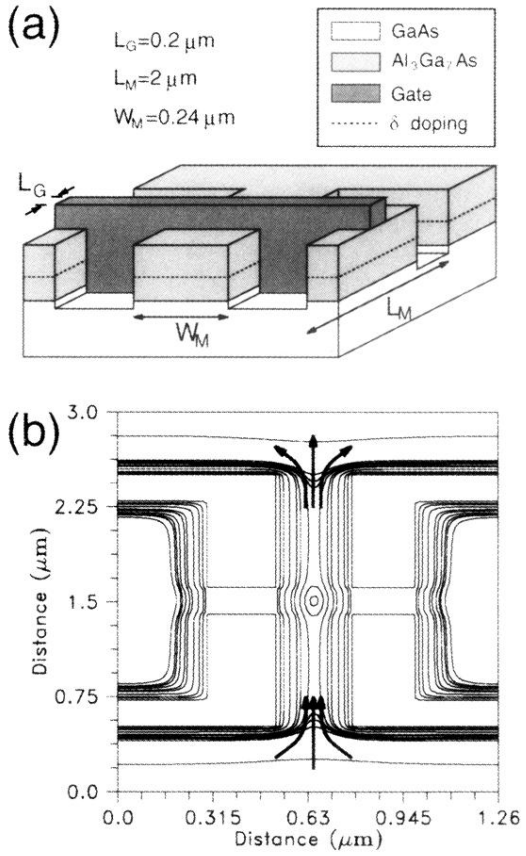

FIG. 1. (a) Schematic configuration for the experimental planar thin-gated quantum-dot device. (b) Potential contours calculated in a plane just below the GaAs-$Al_{0.3}Ga_{0.7}As$ interface. The arrows indicate the direction of current flow.

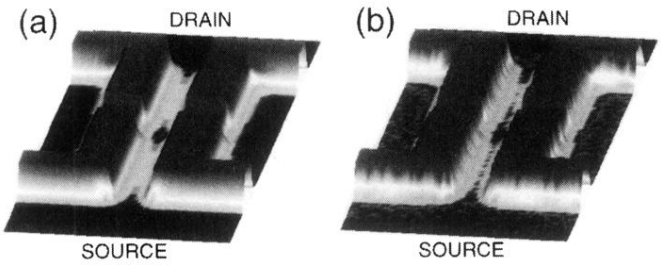

FIG. 5. Theoretical conduction-band surface plots calculated in a plane just below the GaAs-$Al_{0.3}Ga_{0.7}As$ interface (a) using the VCA and (b) with the presence of interface and surface disorder. The potential energy scales with the height of the surface and shading is used to discern subtle energy variations. The disordered surface clearly exhibits a mottled texture arising from the disorder and the presence of weakly localized regions in the quasi-1D channel, which activate resonant transport through the device.